RSC Advances

PAPER

View Article Online
View Journal | View Issue

Cite this: *RSC Adv.*, 2017, **7**, 9031

Characterization of the interaction between triclosan and catalase

Luyi Zou,[a] Chenyu Mi,[a] Hongyan Yu,[a] Wenxiu Gu[b] and Yue Teng*[a]

Received 7th November 2016
Accepted 19th January 2017

DOI: 10.1039/c6ra26431j

rsc.li/rsc-advances

Triclosan (TCS), as a kind of broad spectrum antimicrobial agent, is widely used in personal care products. However, its effectiveness and safety are met with much skepticism. High exposure of TCS to the environment poses a potential threat to ecological safety and human health. In this article, we investigated the interaction between TCS and the antioxidant enzyme catalase (CAT) using spectroscopic techniques and molecular docking technologies. The experimental results showed that TCS could bind into the central cavity of CAT with one binding site to form a TCS–CAT complex, and the main force was the hydrophobic effect. The interaction made some changes to the conformation and micro-environment of CAT and inhibited the activity of CAT. This work explored the interaction between TCS and CAT at the molecular level, which could help us to understand the toxicity mechanism of TCS and provide a reference for pollutant toxicity assessments.

1. Introduction

In recent years, public and scientific concern has heightened interest in the occurrence of pharmaceuticals and personal care products (PPCPs) in the environment. As one kind of PPCPs, triclosan (2,4,4′-trichloro-2′-hydroxy diphenyl ether, TCS) is commonly used as a broad-spectrum antimicrobial agent in personal care products, including toothpastes, soaps, cosmetics, and medical disinfectants, as well as in household items.[1,2] On September 2, 2016, the U.S. Food and Drug Administration issued a final rule on TCS, which triggered a heated discussion about the safety of TCS once again. Many studies have reported environmental exposure and risk assessments of TCS. Research has shown that more than 95% of antimicrobial consumer products are washed down after use and treated in municipal sewage treatment facilities.[1,2] However, the sludge adsorption removal of TCS is about 27%, and then TCS is released from the sludge, which implies the continual release of these compounds into the environment.[1] TCS has been found in aquatic environments, terrestrial environments, organisms, and has even been detected in human milk.[3] Studies have shown that TCS has a negative impact on the soil nitrogen cycle and biological community structure.[4,5] In animal experiments, low doses of TCS were ecotoxic to aquatic organisms and also had endocrine disrupting effects in amphibians and fishes.[6–9] Furthermore, research has shown that TCS can cause DNA damage in human normal stem cells, and has an obvious time–effect relationship.[10] These studies concluded that risk assessments and toxicity information for TCS were significant and urgently needed. Researchers have put much effort into animal level and cell level experiments to explore the toxicity effects of TCS, however, studies at the molecular level for the evaluation of TCS are not clear yet, and this needs to be further researched.

A pollutant's exposure to the environment could cause diseases, and many studies have shown that oxidative stress is related to diseases. In contrast, an antioxidant system could repair the oxidative damage and maintain the dynamic balance of redox reactions in an organism.[11] Investigating the interactions of pollutants and antioxidants has been an important topic. Chen *et al.* have investigated the interaction between TCS and human serum albumin.[12] But research on TCS and antioxidases hasn't been carried out. Catalase (CAT) is one kind of antioxidant enzyme, and has the ability to decompose H_2O_2 into harmless water and oxygen,[13] so as to avoid organism oxidation injury.[14] In this work, the interaction mechanism of TCS with CAT was explored. The binding constants, the number of binding sites and the binding forces of the interaction were investigated by fluorescence measurements. Through molecular docking, spectroscopic analyses, and determination of enzyme activity, we can obtain information about the precise binding site of TCS on CAT, and the conformational and enzymatic changes of CAT by TCS. This work can provide the basic data for understanding the enzyme toxicity of TCS to CAT and the human health risk of TCS *in vivo*.

[a]*Jiangsu Key Laboratory of Anaerobic Biotechnology, School of Environmental and Civil Engineering, Jiangnan University, 1800# Lihu Avenue, Wuxi 214122, PR China. E-mail: tengyue@jiangnan.edu.cn*

[b]*School of Chemical and Material Engineering, Jiangnan University, 1800# Lihu Avenue, Wuxi 214122, PR China*

2. Experimental section

2.1. Reagents

CAT (bought from Beijing BioDee Biotechnology Co. Ltd, and extracted from a bovine liver) was dissolved in 100 mL of ultrapure water to form a 1.0×10^{-5} M solution, and then preserved at 0–4 °C and diluted as required.

TCS (1×10^{-3} M) was prepared as a stock solution by dissolving 0.03 g of TCS (bought from Shanghai Macklin Biochemical Co., Ltd) in 100 mL of ultrapure water with the addition of NaOH (1.0 M) due to TCS being more soluble in alkaline solutions.

Phosphate buffer (0.2 M, a mixture of $NaH_2PO_4 \cdot 2H_2O$ and $Na_2HPO_4 \cdot 12H_2O$, pH 7.6) was used to control the pH of the solutions. $NaH_2PO_4 \cdot 2H_2O$ and $Na_2HPO_4 \cdot 12H_2O$ were of analytical reagent grade, and obtained from Sinopharm Chemical Reagent Co., Ltd.

H_2O_2 (1×10^{-2} M) was prepared by pipetting 50 μL of 30% H_2O_2 (10 M, obtained from Sinopharm Chemical Reagent Co., Ltd) and diluting it with ultrapure water to 50 mL.

Ultrapure water (18.25 MΩ) was used throughout the experiments.

2.2. Apparatus and methods

All fluorescence spectra were taken using an RF-5301 PC fluorescence spectrophotometer (SHIMADZU, Japan) equipped with a 1 cm cell.

UV-visible absorption spectra were recorded on a UV-2700 spectrophotometer (SHIMADZU, Japan) with 1 cm quartz cells.

Circular dichroism (CD) measurements were performed on a MOS 450 spectrometer (Bio Logic, France) in a 1 cm cell.

The absorbance of H_2O_2 was measured on a UV-1100 model spectrophotometer (MAPADA, China) with 1 cm quartz cells.

The pH values were measured with a STARTER 300 OHAUS.

2.2.1. Fluorescence measurements. The fluorescence measurement samples were prepared as follows: 1.0 mL of 0.2 M phosphate buffer (pH 7.6) and 1.0 mL of CAT (1×10^{-5} M) were added to each 10 mL test tube; then different amounts of the stock solution of TCS (1×10^{-3} M) were added to give a concentration ranging from 0 to 6×10^{-6} M. The fluorescence spectra were then measured under the following conditions: excitation at 280 nm and an emission wavelength of 295–470 nm. The synchronous fluorescence spectra were measured at $\lambda_{ex} = 270$ nm, $\Delta\lambda = 15$ nm and $\lambda_{ex} = 240$ nm, $\Delta\lambda = 60$ nm.

2.2.2. UV-visible absorption measurements. The absorption spectra were taken using a UV-2700 spectrophotometer (SHIMADZU, Japan) equipped with 1.0 cm quartz cells. The slit width was set at 4 nm. The wavelength range was 190–325 nm.

2.2.3. Circular dichroism (CD) measurements. CD spectra were recorded on a MOS 450 spectrometer (Bio-Logic, France) using a 1 cm cell. The scanning range was 190–255 nm, the bandwidth was 4 nm, and the scanning speed was 1 nm/2 s. The circular dichroism spectroscopic data was analyzed using the online server DICHROWEB to calculate the protein secondary structure changes.[15]

2.2.4. Molecular docking investigation. Molecular calculations were carried out on the bovine liver CAT protein model (PDB code 1TGU) using AutoDock 4.2 (developed by The Scripps Research Institute, USA).[16,17] The ligand molecule triclosan (ID 2216) was downloaded from the ZINC database.[18] With the aid of AutoDock tools, the ligand root of TCS was detected and the rotatable bonds were defined. H_2O molecules were removed from the CAT model and all hydrogen atoms and computed Gasteiger charges were added. The grid box options were set to 126 points × 126 points × 126 points per map with 1.000 angstrom spacing. The Lamarckian genetic algorithm search method was applied for docking simulations. Each run of the docking experiment was set to terminate after a maximum of 250 000 energy evaluations, and the population size was set to 150. Finally, we selected the lowest binding energy conformation to analyze further.

2.2.5. Enzymatic activity assay. The activity of CAT under the influence of different concentrations of TCS was measured at 240 nm on a UV-1100 model spectrophotometer (MAPADA) at room temperature in a 1.0 cm cuvette, using H_2O_2 as the substrate. CAT catalyzed the decomposition of H_2O_2 and decreased the absorbance. The inhibition rate of CAT activity was calculated using the following equation:

$$\text{Inhibition rate} = \frac{\Delta A_1}{\Delta A_2} \times 100\% \quad (1)$$

where ΔA_1 and ΔA_2 are the reduction of the absorption value at 240 nm within 2 minutes after the addition of CAT with or without TCS.

3. Results and discussion

3.1. Characterization of the interaction of TCS with CAT by fluorescence measurements

3.1.1. Fluorescence quenching. We utilized the fluorescence technique to study the interactions between CAT and TCS, including the quenching mechanism, binding constants and binding sites. From Fig. 1, we know that the fluorescence intensity (F) of CAT decreased regularly with an increasing

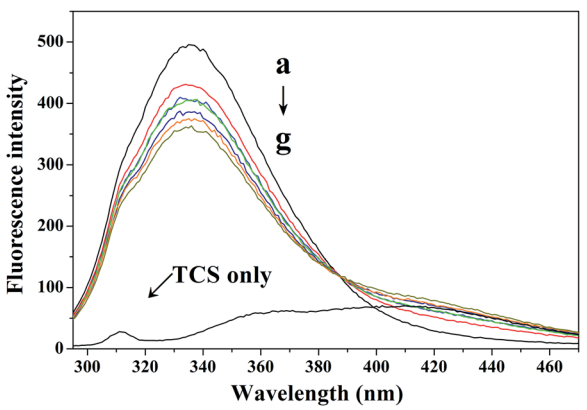

Fig. 1 Effect of TCS on the fluorescence of CAT. Conditions: CAT: 1×10^{-7} M; TCS ($\times 10^{-6}$ M): (a) 0, (b) 1, (c) 2, (d) 3, (e) 4, (f) 5, and (g) 6. TCS only: 1×10^{-4} M; pH 7.4; $T = 300$ K.

concentration of TCS, indicating that TCS had a fluorescence quenching effect on CAT.

A quenching mechanism includes static and dynamic quenching. For dynamic quenching, a higher temperature results in a larger diffusion coefficient and an increase in the dynamic quenching constants. In contrast, an increased temperature can decrease the stability of complexes, and lower the value of the static quenching constants.[19]

To confirm the quenching mechanism, the fluorescence quenching data were analyzed according to the Stern–Volmer equation.[20]

$$\frac{F_0}{F} = 1 + K_{sv}[Q] = 1 + k_q\tau_0[Q] \quad (2)$$

where F_0 and F are the fluorescence intensities in the absence and presence of the quencher. K_{sv} is the Stern–Volmer quenching constant, [Q] is the concentration of the quencher, k_q is the quenching rate constant of the biological macromolecule, and τ_0 is the fluorescence lifetime in the absence of the quencher.

The Stern–Volmer plots are presented in Fig. 2, and the fluorescence data were analyzed according to F_0/F *versus* [Q] at 300 and 320 K. We can determine K_{sv} by a linear regression plot of F_0/F against [Q] using eqn (2). Because the fluorescence lifetime of the biopolymer (τ_0) is 1×10^{-8} s,[21] the value of k_q can be obtained.

The maximum scatter collision quenching constant of various quenchers with a biopolymer is 2.0×10^{10} L mol^{-1} s^{-1}.[22] As is shown in Table 1, the K_{sv} values decreased with increasing temperature and k_q was greater than 2.0×10^{10} L mol^{-1} s^{-1}. So we can conclude that overall quenching was dominated by a static quenching mechanism forming a TCS–CAT complex.

3.1.2. Association constants and the number of binding sites. Through the former analysis, the quenching mechanism was determined to be a static quenching mechanism, and knowing this we can calculate the other constants through the following formula.[23]

$$\lg\frac{(F_0 - F)}{F} = \lg K_a + n \lg[Q] \quad (3)$$

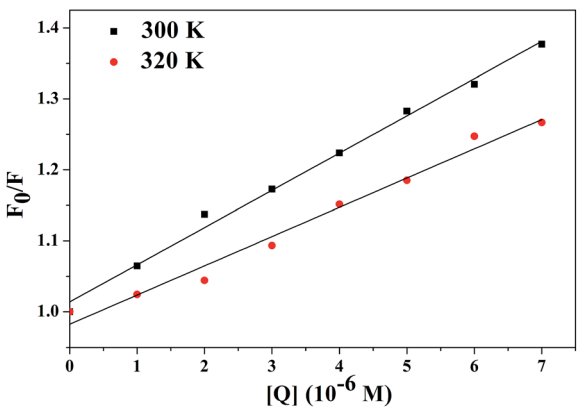

Fig. 2 Stern–Volmer plots for the quenching of CAT by TCS at 300 K and 320 K.

Table 1 Stern–Volmer quenching constants for the interaction of TCS with CAT at 300 K and 320 K

T (K)	K_{sv}	k_q ($\times 10^{12}$ L mol^{-1} s^{-1})	R^a	S.D.^{b}
300	5.2	5.2	0.9933	0.01634
320	4.1	4.1	0.9799	0.02228

^{a} R: the correlation coefficient. ^{b} S.D.: the standard deviation for the K_{sv} values.

where F_0, F, and [Q] are the same as in eqn (2), K_a is the binding constant, and n is the number of binding sites per CAT molecule. The values of n and K_a are shown in Table 2, and we can see that the number of binding sites n is approximately equal to 1, indicating that TCS is bound into CAT by one site.

3.1.3. Thermodynamic parameters and binding forces. The acting forces between small organic molecules and biomolecules include hydrophobic interaction forces, van der Waals interactions, electrostatic forces and hydrogen bonds.[24] When the temperature range is not too wide, we can regard the interaction enthalpy change (ΔH) as a constant. The enthalpy change (ΔH), free-energy change (ΔG) and entropy change (ΔS) for the interaction between TCS and CAT were calculated according to the Van't Hoff equation (eqn (4)) and the thermodynamic equation (eqn (5)).

$$\ln\left(\frac{K_a}{K_b}\right) = \left(\frac{1}{T_1} - \frac{1}{T_2}\right)\left(\frac{\Delta H}{R}\right) \quad (4)$$

$$\Delta G = \Delta H - T\Delta S = -RT \ln K_a \quad (5)$$

where K_a and K_b are the binding constant at T_1 and T_2 and R is the universal gas constant. From Table 2, we can conclude from the positive ΔH and ΔS that hydrophobic interaction forces played a leading role in the interaction.[25] And the negative ΔG implies that the interaction between CAT and TCS was spontaneous.

3.1.4. Identification of the binding sites on CAT. Molecular docking methods were adopted to identify the binding sites of TCS to CAT (Fig. 3). From Fig. 3A, we can see that TCS does not bind into the CAT active sites directly but binds into the cavity of the enzyme, locating among the four subdomains of CAT. The amino acid residues lining the binding site are PRO390 and HIS363 of chain A; ILE68, PRO69, PRO390, PRO367, ARG364, LEU365, and GLY366 of chain B; PRO69 and HIS363 of chain C; and PRO390, PRO367, GLY366, ARG362, and MET391 of chain D. The essential forces that drive the TCS molecule to bind to the site are hydrophobic interaction forces and there is no hydrogen bonding between TCS and CAT.

3.2. Investigation of CAT conformation changes

3.2.1. UV-vis absorption spectroscopy. UV-visible absorption measurements can be used to explore the structural changes of proteins and to investigate protein–ligand complex formation. The UV-vis absorption spectra of CAT in the presence and absence of TCS are shown in Fig. 4.

Table 2 Binding parameters and thermodynamic parameters for the interaction of TCS with CAT at 300 K and 320 K

T (K)	K_a ($\times 10^5$ M^{-1})	n	R^a	ΔH (kJ mol^{-1})	ΔS (J mol^{-1} K^{-1})	ΔG (kJ mol^{-1})
300	0.501	0.8575	0.9820	213.45	787.83	−22.9
320	0.455	1.3118	0.9814		786.09	−38.1

[a] R: the correlation coefficient.

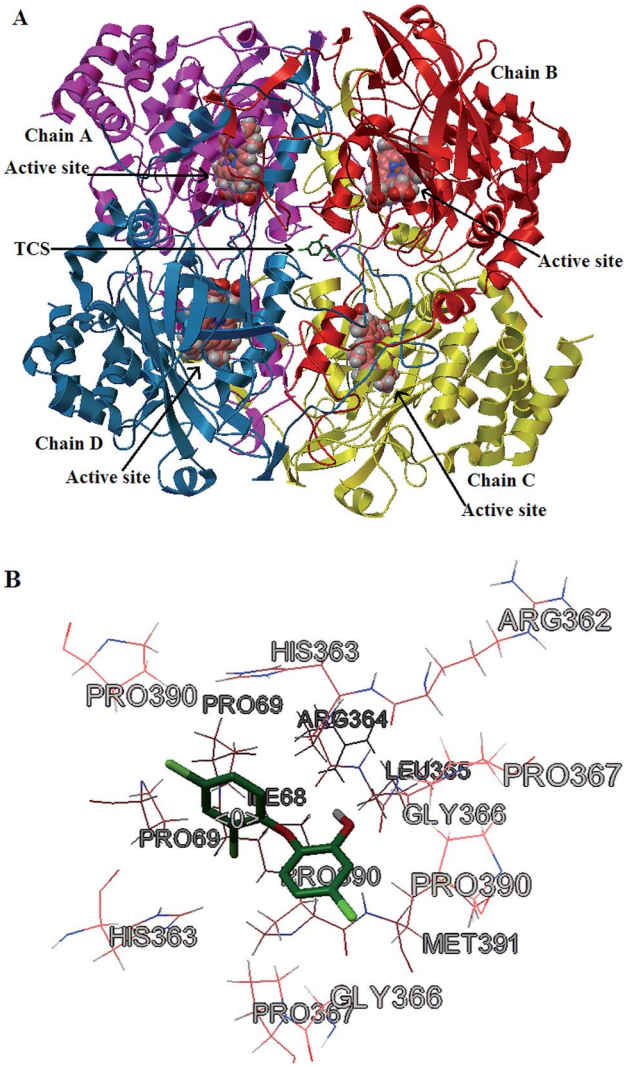

Fig. 3 (A) Molecular docking results of TCS and CAT generated using AutoDock. (B) Detailed illustration of the binding mode between TCS and the residues of CAT.

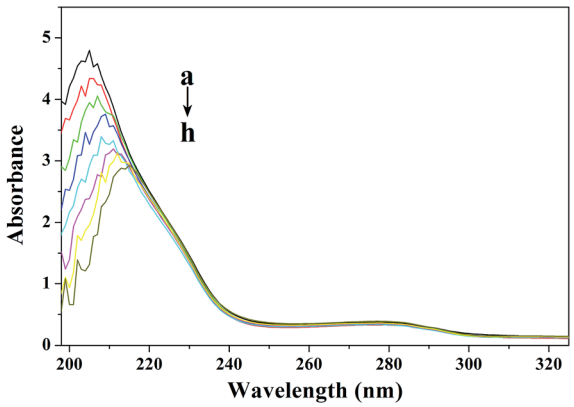

Fig. 4 UV-vis spectra of CAT in the presence of different concentrations of TCS. Conditions: CAT: 1×10^{-6} M, TCS ($\times 10^{-5}$ M): (a) 0, (b) 1, (c) 2, (d) 3, (e) 4, (f) 5, (g) 6, and (h) 7. pH 7.4; $T = 300$ K.

The strong absorption peak at about 205 nm reflects the framework conformation of the protein.[26] With the increasing concentration of TCS, the absorbance of CAT decreased and the maximum peak position of TCS–CAT was red-shifted, indicating that the interaction between TCS and CAT resulted in the loosening and unfolding of the protein skeleton.

3.2.2. Synchronous fluorescence. Synchronous fluorescence spectroscopy can provide information on molecular microenvironments, especially in the vicinity of fluorophore functional groups. The spectrum is obtained through the simultaneous scanning of the excitation and emission monochromators while maintaining a constant wavelength interval between them. When the wavelength intervals ($\Delta\lambda$) are stabilized at 15 or 60 nm, the synchronous fluorescence gives the characteristic information of tyrosine (Tyr) or tryptophan (Trp) residues, respectively, and the shifts in the emission maximum reveal the changes in the polarity of their environment.[27]

The synchronous fluorescence spectra of CAT at two different wavelength intervals are shown in Fig. 5. It can be seen in Fig. 5A that the maximum emission wavelength had a small blue shift when $\Delta\lambda$ was 15 nm, revealing that the hydrophobicity of the Tyr residues increased, and the polarity of the microenvironment around the Tyr residues decreased. In Fig. 5B, the position of the maximum emission of the Trp residues doesn't change obviously, which indicates that TCS had little effect on the microenvironment of the Trp residues in CAT.

3.2.3. Circular dichroism. To evaluate the possible influence of TCS binding on the secondary structure of CAT, CD measurements were performed (Fig. 6) and we have analyzed the CD spectra using the CD analysis of four secondary structures: α-helices, β-sheets, β-turns and unordered structures (Table 3). With the addition of TCS to CAT (5 : 1 and 25 : 1), the α-helix content of CAT decreased from 34.3% to 20.6% and 20.4%, and the β-sheet content increased from 11.3% to 24.5% and 25.3%. Obviously, TCS transformed some α-helices into β-

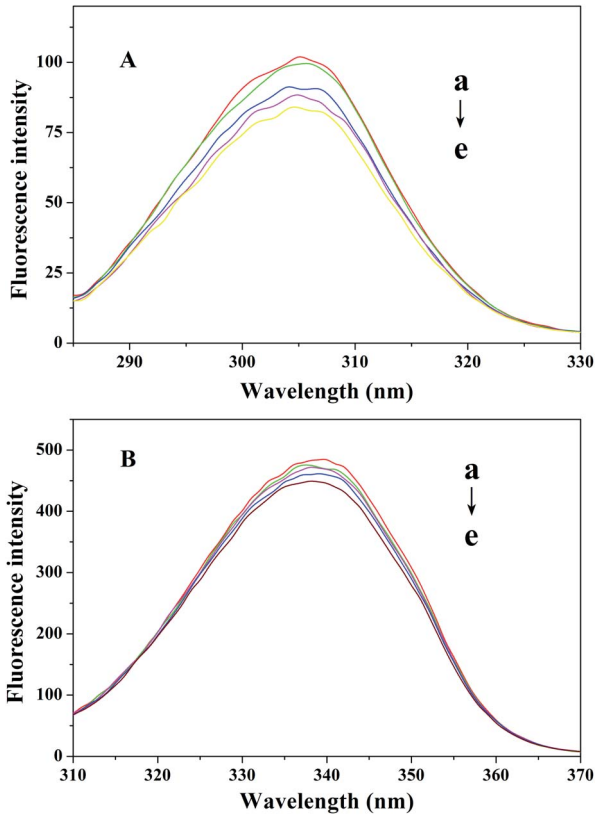

Fig. 5 Synchronous fluorescence spectra of CAT. (A) $\Delta\lambda = 15$ nm and (B) $\Delta\lambda = 60$ nm. Conditions: CAT: 1.0×10^{-6} M; TCS (a–e) ($\times 10^{-6}$ M): 0, 1, 2, 3, and 4.

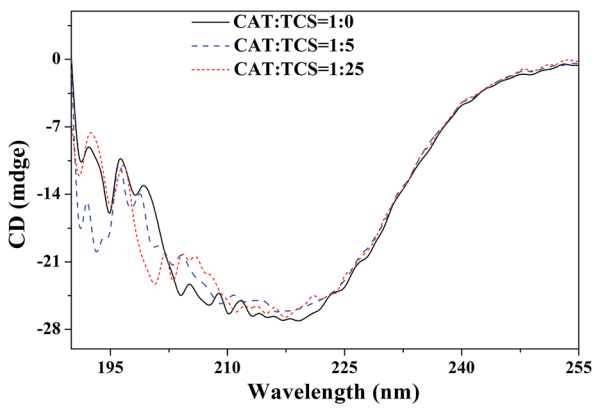

Fig. 6 CD spectra of CAT and the CAT–TCS system. Conditions: CAT: 2×10^{-7} M; TCS concentrations in the CAT–TCS system were 0, 1×10^{-6} M, and 5×10^{-6} M.

sheets and random coils and TCS induced these changes in the secondary structure of CAT.

3.3. Effect of TCS on CAT activity

The effect of different concentrations of TCS on the relative CAT activity is shown in Fig. 7. We can see that the relative CAT activities are reduced to 85%, 76%, and 74% after reaction with

Table 3 Effect of TCS on the percentage of secondary structural elements in CAT

	Secondary structural elements in CAT			
Molar ratio CAT to TCS	α-Helix (%)	β-Sheet (%)	β-Turns (%)	Unordered (%)
1 : 0	34.3	11.3	23.3	32.3
1 : 5	20.6	24.5	19.3	38.6
1 : 25	20.4	25.3	19.3	39.2

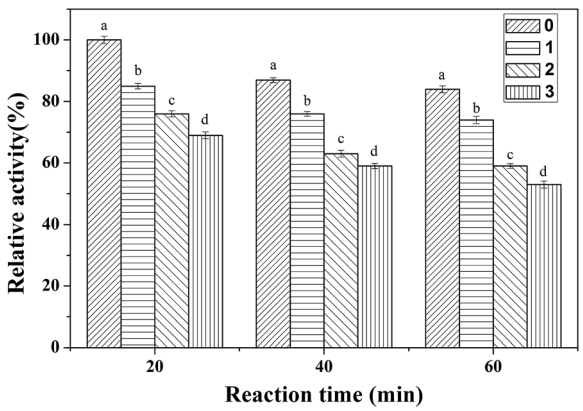

Fig. 7 The effect of TCS on CAT activity at different concentrations and different reaction times. Conditions: pH 7.6; $T = 298$ K, CAT: 1×10^{-7} M; TCS ($\times 10^{-5}$ M): (0) 0; (1) 1; (2) 2; and (3) 3. The lowercase letters a, b, c, and d in the same reaction time indicate significant differences ($P < 0.05$).

1, 2 and 3 ($\times 10^{-5}$ M) TCS for 20 minutes. As the reaction happened, the relative activities were reduced to 74%, 59% and 53% after 1 h of reaction. It's revealed that both the reaction time and the concentration of TCS had a notable impact on the CAT activity. Combined with the previous experimental results and molecular docking analysis, we can conclude that although the TCS molecule did not directly bind into the CAT active site, it influenced the microenvironment around the active site, resulting in the reduction of CAT activity.

4. Conclusions

In this paper, we simulated physiological conditions to explore the interactions between the widely used broad-spectrum antimicrobial agent TCS and the antioxidant enzyme CAT. The spectroscopic analysis and thermodynamic results indicated that the TCS molecule can spontaneously bind with CAT to form a TCS–CAT complex with one binding site mainly through hydrophobic interaction forces. TCS could also obviously change the skeleton and the secondary structure of CAT. According to molecular docking simulation analysis and enzyme activity experiments, we found that the exact binding site of TCS with CAT was the central cavity, and TCS influenced the microenvironment of the active site and further induced the inhibition of CAT activity. This research can provide data support for the comprehensive evaluation of TCS and act as

a reference for other environmental pollutant toxicity mechanism research.

Acknowledgements

The work is supported by the National Nature Science Foundation of China (NSFC, 21307043), the China Postdoctoral Science Foundation (2016M590411), the Postdoctoral Science Foundation of Jiangsu Province (1601230C) and the Independent Research Project of Jiangnan University (JUSRP11525).

References

1 K. Bester, *Water Res.*, 2003, **37**, 3891–3896.
2 D. Sabaliunas, S. F. Webb, A. Hauk, M. Jacob and W. S. Eckhoff, *Water Res.*, 2003, **37**, 3145–3154.
3 M. Adolfsson-Erici, M. Pettersson, J. Parkkonen and J. Sturve, *Chemosphere*, 2002, **46**, 1485–1489.
4 N. J. Waller and R. S. Kookana, *Environ. Toxicol. Chem.*, 2009, **28**, 65–70.
5 H. Svenningsen, T. Henriksen, A. Priemé and A. R. Johnsen, *Environ. Pollut.*, 2011, **159**, 1599–1605.
6 R. Reiss, N. Mackay, C. Habig and J. Griffin, *Environ. Toxicol. Chem.*, 2002, **21**, 2483–2492.
7 C. M. Foran, E. R. Bennett and W. H. Benson, *Mar. Environ. Res.*, 2000, **50**, 153–156.
8 S. L. Fraker and G. R. Smith, *Environ. Toxicol.*, 2004, **19**, 250–256.
9 N. Matsumura, H. Ishibashi, M. Hirano, Y. Nagao, N. Watanabe, H. Shiratsuchi, T. Kai, T. Nishimura, A. Kashiwagi and K. Arizono, *Biol. Pharm. Bull.*, 2005, **28**, 1748–1751.
10 L. Linpeng, M. Huimin, H. Junjie, L. Yuhua, W. Yipei, S. Guoying and F. Mojia, *Journal of Ecological Environment*, 2010, **19**, 2897–2901.
11 J. Limón-Pacheco and M. E. Gonsebatt, *Mutat. Res., Fundam. Mol. Mech. Mutagen.*, 2008, **674**, 137–147.
12 J. Chen, X. Zhou, Y. Zhang, Y. Zi, Y. Qian, H. Gao and S. Lin, *Environ. Sci. Pollut. Res. Int.*, 2011, **19**, 2528–2536.
13 D. Giustarini, I. Dalledonne, D. Tsikas and R. Rossi, *Crit. Rev. Clin. Lab. Sci.*, 2009, **46**, 241–281.
14 X. Zhang and J. Jin, *J. Mol. Struct.*, 2008, **882**, 96–100.
15 L. Whitmore and B. A. Wallace, *Biopolymers*, 2008, **89**, 392–400.
16 S. Ardissone, E. Laurenti, P. Frendo, E. M. Ghibaudi and A. Puppo, *JBIC, J. Biol. Inorg. Chem.*, 2005, **10**, 813–826.
17 G. M. Morris, R. Huey, W. Lindstrom, M. F. Sanner, R. K. Belew, D. S. Goodsell and A. J. Olson, *J. Comput. Chem.*, 2009, **30**, 2785–2791.
18 J. J. Irwin, T. Sterling, M. M. Mysinger, E. S. Bolstad and R. G. Coleman, *J. Chem. Inf. Model.*, 2012, **52**, 1757–1768.
19 D. Lu, X. Zhao, Y. Zhao, B. Zhang, B. Zhang, M. Geng and R. Liu, *Food Chem. Toxicol.*, 2011, **49**, 3158.
20 S. Soares, A. Nuno Mateus and V. D. Freitas, *J. Agric. Food Chem.*, 2007, **55**, 6726–6735.
21 J. R. Lakowicz and G. Weber, *Biochemistry*, 1973, **12**, 4161–4170.
22 Z. Chi, R. Liu and H. Zhang, *Biomacromolecules*, 2010, **11**, 2454–2459.
23 X. Zhao, R. Liu, Z. Chi, Y. Teng and P. Qin, *J. Phys. Chem. B*, 2010, **114**, 5625–5631.
24 Z. Chi and R. Liu, *Biomacromolecules*, 2011, **12**, 203–209.
25 P. D. Ross and S. Subramanian, *Biochemistry*, 1981, **20**, 3096–3102.
26 D. Li, B. Ji and J. Jin, *J. Lumin.*, 2008, **128**, 1399–1406.
27 J. Zhu, X. Zhang, D. Li and J. Jin, *J. Mol. Struct.*, 2007, **843**, 38–44.